Accepted Manuscript

The auditory evoked-gamma response and its relation with the N1m.

Caroline Witton, Mark A. Eckert, Ian M. Stanford, Lauren E. Gascoyne, Paul L. Furlong, Siân F. Worthen, Arjan Hillebrand

PII: S0378-5955(17)30082-5

DOI: 10.1016/j.heares.2017.02.016

Reference: HEARES 7333

To appear in: *Hearing Research*

Received Date: 6 April 2015

Revised Date: 13 July 2016

Accepted Date: 3 February 2017

Please cite this article as: Witton, C., Eckert, M.A., Stanford, I.M., Gascoyne, L.E., Furlong, P.L., Worthen, S.F., Hillebrand, A., The auditory evoked-gamma response and its relation with the N1m., *Hearing Research* (2017), doi: 10.1016/j.heares.2017.02.016.

The auditory evoked-gamma response and its relation with the N1m.

Caroline Witton[a*], Mark A. Eckert[b], Ian M. Stanford[a], Lauren E. Gascoyne[a], Paul L. Furlong[a], Siân F. Worthen[a], Arjan Hillebrand[c]

[a]Aston Brain Centre, Aston University, Birmingham, B4 7ET, UK

[b]Department of Otolaryngology-Head and Neck Surgery, Medical University of South Carolina, Charleston, South Carolina, USA

[c]Department of Clinical Neurophysiology and Magnetoencephalography Center, VU University Medical Center, 1081 HV Amsterdam, the Netherlands

*corresponding author:

c.witton@aston.ac.uk

Aston Brain Centre, Aston University,

Birmingham,

B4 7ET, UK

Tel: +44 (0) 121 2044087

Abstract

This study explored the patterns of oscillatory activity that underpin the N1m auditory evoked response. Evoked gamma activity is a small and relatively rarely-reported component of the auditory evoked response, and the objective of this work was to determine how this component relates to the larger and more prolonged changes in lower frequency bands. An event-related beamformer analysis of MEG data from monaural click stimulation was used to reconstruct volumetric images and virtual electrode time series. Group analysis of localisations showed that activity in the gamma band originated from a source that was more medial than those for activity in the theta-to-beta band, and virtual-electrode analysis showed that the source of the gamma activity could be statistically dissociated from the lower-frequency response.

These findings are in accordance with separate functional roles for the activity in each frequency band, and provide evidence that the oscillatory activity that underpins the auditory evoked response may contain important information about the physiological basis of the macroscopic signals recorded by MEG in response to auditory stimulation.

Keywords

beamformer, cortex, magnetoencephalography, oscillations

1 Introduction

The auditory N1, termed the N1m in MEG data, is a large evoked response elicited by the onset of a sound and originating in auditory cortex (Näätänen & Picton, 1987). It is relatively slow and prolonged, consisting of a series of waves between about 75 and 120 ms following stimulation (see Figure 1). Less frequently-reported is the auditory evoked-gamma response, which is typically 10-15 times smaller than the N1 (Jacobson & Fitzgerald, 1997). Sometimes observed as 'notching' superimposed on the slow waves of the N1, it is most easily viewed in data that has been high-pass filtered to exclude frequencies below 30 Hz (Jacobson & Fitzgerald, 1997; Pantev, 1995). Dipole-modelling (Pantev, 1995) and cortical surface recordings (Jacobson & Henderson, 1998) have suggested that the auditory evoked-gamma response originates from a separate source to the slower N1 and may therefore be functionally different. The objective of this study was to characterize the spatio-temporal characteristics of the evoked oscillatory activity during auditory processing.

Gamma-band activity, here classified as synchronous neuronal oscillatory activity at 30 - 70 Hz, results from the coordinated interaction between excitatory and inhibitory neurons (Bartos, Vida, & Jonas, 2007) and is functionally widespread in the brain. It is predominant during high attentional states, and induced (i.e. stimulus-related but not time-locked) gamma band changes in particular have been implicated in high-level cortical processes such as sensory perception (Engel & Singer, 2001; Gray & Singer, 1989; Singer, 1993), learning and memory processes (Buzsáki & Chrobak, 1995; Lisman & Idiart, 1995; Lisman, 1999), memory storage and retrieval (Colgin & Moser, 2010) as well as object recognition and language perception (Crone, Boatman, Gordon, & Hao, 2001; Kaiser, Hertrich, Ackermann, Mathiak, & Lutzenberger, 2005). Evoked, rather than induced, gamma activity is most commonly observed in auditory cortex. The steady-state evoked response to an amplitude-modulated tone is strongest when the rate of modulation falls in the gamma band (40 Hz; e.g. Rees, Green, & Kay, 1986; Ross et al., 2000), indicating that auditory cortical networks are optimised to oscillate in this range. However this is a *driven* response and most likely differs mechanistically from

the brief burst of intrinsic gamma oscillations that accompanies the N1m. The evoked gamma activity that follows a transient auditory stimulus such as a tone or click is known to be affected in terms of both amplitude and connectivity patterns by task conditions (e.g. Mulert et al., 2007, Polomac et al., 2015), implying that it has functional significance.

Hierarchical models of auditory cortical processing suggest that the holistic perception of auditory 'objects' (acoustic events or sources; see Griffiths & Warren 2004) emerges from serial processing in a sequence of brain areas beginning with those lying within Heschl's gyrus, and progressing to areas in planum temporale and STS where more complex analysis of stimulus features takes place (Kumar, Stephan, Warren, Friston, & Griffiths, 2007). Such models underline the need for effective communication between sub-regions within Heschl's gyrus, planum temporale, and beyond, as well as the dynamic recruitment of neurons within these sub-regions to form local networks. Oscillatory dynamics, widely implicated in communication within networks (Wang, 2010) can therefore be hypothesised to play a central role in facilitating and controlling the communication between regions within auditory cortex. For example, within auditory cortex, persistent gamma oscillations have been observed in superficial layers (Traub, Bibbig, LeBeau, Cunningham, & Whittington, 2005) while slower oscillations, such as those in the beta-band or lower, which can synchronise over longer delays, are thought to enable communication between regions that are spatially more separated (Kopell, Ermentrout, Whittington, & Traub, 2000). If patterns of oscillatory activity can be effectively localised and distinguished at the macroscopic level, then this will provide important opportunities to further explore the cortical pathways involved in auditory perception.

An early MEG study using the single-dipole modelling approach established that this response originates in supra-temporal auditory cortex, adjacent to but 'deeper' than the N1m response (Pantev et al., 1991). Important recent developments in MEG data analysis, using whole-head MEG systems with dense coverage, have provided new methods, such as beamformers (Hillebrand, Singh, Holliday, Furlong, & Barnes, 2005; Vrba & Robinson, 2001), that are particularly suited to the study of brain responses that are specifically defined in terms of their frequency

characteristics (like gamma-band activity). Beamformers provide several additional benefits over more traditional dipole-fitting techniques, especially the absence of any need for *a-priori* assumptions about the number of sources (van Veen et al. 1997), and their ability to significantly enhance the signal-to-noise ratio of the data (Adjamian et al., 2009). The use of such techniques therefore allows for a more detailed characterisation of the low-amplitude evoked-gamma response, and should potentiate our understanding of its functional role. In this study, we used beamformer analysis of MEG data to characterize the spatio-temporal properties of the oscillatory changes that underpin the gamma-band and lower-frequency components of the auditory evoked response, with the objective of gaining insight into their functional relation within auditory cortex.

2 Materials and Methods

2.1 Participants

11 adults (7 females; age-range 26-71 years), with no reported neurological or audiological problems, took part in the study. Participants were recruited from an ad-hoc population of university staff and graduate students. The study was conducted in accordance with the Declaration of Helsinki and with the consent of the local Ethics committee.

2.2 Stimuli

The stimuli were a train of 200 acoustic clicks with an average inter-stimulus interval of 1200 ms, randomly jittered by plus or minus 200 ms and presented using a PC running Presentation® software (version 0.7, www.neurobs.com). These were delivered monaurally to the left and right ears in separate recordings (in counterbalanced order across participants), through echoless plastic tubing and foam ear-tips at a comfortable, calibrated, 50dB hearing level.

2.3 MEG data collection

Data were recorded using a 275-channel whole-head CTF MEG system (CTF Systems, Port Coquitlam, Canada), while participants were seated with their eyes open in a dimly lit magnetically shielded room, watching a silent video to maintain alertness. The measurements for this study took less than 5 minutes and formed part of a longer recording session involving auditory measurements for other

studies. MEG data were recorded using synthetic third-order gradiometers (Vrba et al., 1999), sampled at 600 Hz with an anti-aliasing filter of 300 Hz, power-line filtered, and subdivided into epochs starting 500 ms before each click to 500 ms following each click. Each epoch was baseline-corrected by the mean amplitude of the 500-ms pre-stimulus period. The epochs were stringently screened visually for physiological artefacts such as those arising from eye-blinks and muscle activity, resulting in the removal of on average 32 epochs per dataset.

Source modelling was achieved by using an event-related beamformer (Cheyne, Bostan, Gaetz, & Pang, 2007). MEG data were spatially coregistered with the individual's structural MRI using a modification of the surface-matching method described by Adjamian et al (2004), and a multi-sphere head model (Huang, Mosher, & Leahy, 1999) was derived from each participant's outer skull surface. Noise-normalised weights were computed from the un-averaged data, using a time window from 0 to 200 ms post-trigger, for two separate frequency bands: 4-30 Hz ('theta-to-beta') and 30-70 Hz ('gamma'). While power estimates for the lowest frequencies may have been sub-optimal due to the use of brief time windows for the covariance estimation (Brookes et al., 2008), our inclusion of the theta-band allowed us to capture some of the slower components associated with the traditionally-defined N1m response. The weights were applied to the averaged data, which had been filtered into the same frequency band, for the time-points of interest – the largest peak of the auditory evoked-gamma response and the N1m for each individual and hemisphere, to yield a volumetric image.

The co-ordinates of peak voxels were transformed to Talairach co-ordinates by manual identification of key landmarks (the anterior and posterior commissures; Talairach & Tournoux, 1988) using MRI3dX software (v. 7.63) to enable comparison between individuals. Activations were accepted if they fell broadly within, or close to, the superior surface of the temporal lobe, near or posterior to Heschl's gyrus. They had to fall between co-ordinates of -10 and 30 in the Z-direction (inferior-superior) and 0 and -60 mm in the X-direction (anterior-posterior), but were not restricted in the Y-direction except that they had to fall within the expected hemisphere. They also had to fall

within the 5 maximal peaks obtained by the analysis (we allowed the rank of the peak to vary because, although we expected auditory cortical activation to be the most significant activity observed in this paradigm, localisable artefacts, other task-related activity, or spurious activations (Quraan & Cheyne, 2010) could also cause peaks in the image, such that we would have missed genuine activation if we had only selected the main peak). The pseudo-Z score for each accepted peak voxel was also recorded. Full-width half-maximum (FWHM) analyses of peak smoothness were computed according to the method described by Barnes and Hillebrand (2003).

2.4 Virtual Electrode (VE) Analysis

VE time series were constructed (Hillebrand et al., 2005; Robinson & Vrba, 1999) to allow analysis of the spectro-temporal properties of evoked activity at the sources identified in the volumetric images, using the co-ordinates of each individual's response. The previously computed noise-normalised weights were multiplied by the averaged, unfiltered sensor data to produce virtual electrode time series. Time-frequency spectrograms were created using Morlet wavelets with a width of 7 cycles. For comparison of evoked response time series in the virtual electrode data at each cortical location of interest, the time series were both filtered into the theta-to-beta band and, separately, the gamma band. Each was then individually scaled relative to one standard deviation of the evoked-response time series in its pre-stimulus baseline period (i.e., 1 standard deviation of pooled sample-points). This scaling allowed comparison of evoked response morphology between source models, despite any differences in overall signal amplitude. Group means and standard deviations were then computed for each filtered, standardised, time series at each cortical location.

2.5 Anatomical Localisation

The mean coordinates for gamma-band and theta-to-beta responses were examined to determine where these responses were localised in auditory cortex. The mean Talairach coordinates defined with MRI3dX were converted to MNI space using the GingerALE MNI2Tal tool (Laird et al.,

2010; Lancaster et al., 2007). These coordinates were then displayed with primary auditory cortex probabilistic maps for the medial to lateral cytoarchitectonic regions Te1.1, Te1.0, and Te1.2 (Morosan et al., 2001). This qualitative examination allowed for further characterization of the spatial separation between the gamma and theta-to-beta responses.

3 Results

3.1 Sensor Data: Relative amplitude and latency in the gamma and theta-to-beta bands.

Figure 1 shows example data from a sensor over the temporal lobe, filtered between 1 and 30 Hz illustrating the N1m response (Fig. 1a), and separately between 30 and 70-Hz illustrating the evoked-gamma response (Fig. 1b). The approximately five-fold difference in amplitude between the responses in each filter-band can be seen by comparing values on the ordinate axes. Table 1 shows the means with standard deviations for the latencies of the peak of each response observed in the sensor data, along with the number of participants showing a discernible response upon which these data are based. For each ear of stimulation, 10 of the 11 participants showed a clear N1m response in the sensor data for the hemisphere contralateral to stimulation (i.e. one did not show a contralateral response for left-ear stimulation, and a different participant did not for right-ear stimulation). The two participants who did not show an N1m response did both show activation in the gamma band. Contralateral gamma-band responses, occurring around 80 ms, were discernible in 8 participants for stimulation in each ear (5 cases with bilateral responses). A subset of participants also showed N1m or gamma-band responses in the hemisphere ipsilateral to stimulation (also shown in Table 1). There were no statistically significant differences between hemispheres in response latency for contralateral or ipsilateral responses, or between contralateral and ipsilateral responses within hemispheres (Wilcoxon ranked pairs, $p > 0.05$).

3.2 Source Models: Spatial Dissociation of Responses

194 There were 10 acceptable contralateral and 4 ipsilateral theta-to-beta sources for left ear
195 stimulation; and 9 contralateral, 8 ipsilateral for right-ear stimulation. A subset of the participants
196 yielded an acceptable source in the gamma band which fell within our region of interest: 6
197 contralateral and 5 ipsilateral following left-ear stimulation, and 8 contralateral and 7 ipsilateral
198 following right-ear stimulation. The following anatomical descriptions and statistical comparisons
199 focus on the contralateral responses, although data for the ipsilateral responses are presented in
200 Table 2 and Figure 2.

201 In the left hemisphere, the mean gamma response was observed on the crown of Heschl's
202 gyrus with at least a 50% probability of falling within cytoarchitectonic region Te1.0 (MNI: -49, -17,
203 8). In contrast, the theta-to-beta response was more lateral than the gamma response and localised
204 to the boundary of regions Te1.2 and Te1.0 (MNI: -58, -20, 13). The right hemisphere mean gamma
205 and theta-to-beta responses were again spatially separated, but both shifted more medially. The
206 mean gamma response was observed in the superior temporal gyrus, inferior to the boundaries
207 Te1.1 and Te1.0 (MNI: 50, -23, 1). The more lateral theta-to-beta response was observed in the
208 planum temporale and at the boundary of Te1.1 and Te1.0 regions (MNI: 53, -23, 9).

209 The spatial variability of the left and right hemisphere localisations, as well as their relative
210 spatial positions, is demonstrated in Figure 2. The 95 % confidence intervals for each mean response
211 have the tendency to be more ovoid in the anterior-posterior (Y) and superior-inferior (Z) directions,
212 compared to the medial-lateral (X) direction. The more consistent localisation in the medial-lateral
213 direction is consistent with the significant difference in the X location between gamma and theta-to-
214 beta responses (across both hemispheres, paired t-test of the gamma vs theta-to-beta X location: $t = 4.36$, $p < 0.001$), but not for the Y and Z locations. Thus, the theta-to-beta responses lie consistently
216 lateral to those in the gamma band.

217

218 <u>3.3 Virtual electrode analysis: Spatiotemporal characteristics of VE time series.</u>

An analysis of the virtual electrode time series was conducted in order to further explore the observation of a spatial separation between responses in the gamma band and the N1m (theta-to-beta) response in the left hemisphere. We reconstructed virtual electrodes for left-hemisphere sources from right-ear stimulation in each frequency band for the 7 participants who showed contralateral activations for right-ear stimulation (i.e. left-hemisphere responses) in both the theta-to-beta and gamma bands, and for right-hemisphere sources for the five participants who showed contralateral activations in both bands for left-ear stimulation (i.e. right-hemisphere responses). The volumetric event-related beamformer localisation relies on filtering both the un-averaged data to produce the weights and the average data to represent the results in a frequency band of interest. However activity falling outside this frequency-band of interest may co-occur at the same location, and we can visualise this by applying the same weights to an average that has not been filtered, or has been filtered in a different frequency band, thereby revealing whether a single location contributes to activity in multiple frequency bands.

Figure 3 shows the data for right-ear stimulation: Figs 3a and 3b show group-averaged spectrograms of the evoked activity at the peak sources for theta-to-beta and gamma activity in the left hemisphere, respectively. A burst of spectral power in each frequency band is clearly visible at both locations, though the relative strength of the activity in the gamma band (i.e. the activity localised by the beamformer) is slightly greater at the gamma location (Fig. 3b) and vice-versa. Figures 3c and 3d compare between the evoked responses at the location of the gamma and the theta-to-beta virtual electrodes. In Fig 3c, both the VE time series are filtered in the theta-to-beta frequency band (4-30 Hz), standardised and averaged across subjects. A clear tri-phasic evoked response is observed for both locations, i.e., for both the source of the peak gamma and the source of the peak theta-to-beta activity, which is consistent with the traditionally-defined N1m shown in Figure 1a. The overall standardised amplitude is larger at the source of the gamma activity (despite the VE having been identified as the strongest source of activity in the theta-to-beta band), though standard error-bars are large, and overlap. The trend towards a difference in amplitude at each

location is likely due to increased inter-individual differences in response timing at the theta-to-beta location (not shown in Figures). Nonparametric Wilcoxon tests confirm that there is no significant difference between the amplitudes at the maxima of the second and third waves ($W(6) = 7$, $p > 0.05$). A small but significant difference (i.e. with greater amplitude at the gamma source) is observed at the earliest wave in the average VE time series, which occurs at around 80 ms ($W(6) = 2$, $p = 0.047$). Figure 3d shows the same VE time series, now filtered in the gamma band (30-70 Hz). A burst of evoked gamma occurs in each location but the amplitude is significantly greater in the virtual electrodes obtained from the maximum of gamma-band activity than in those for the theta-to-beta source ($W(6) = 0$, $p = 0.016$). Therefore, the gamma-band response amplitude is greater at its peak source than at the peak of the lower-frequency activity, whereas the amplitude of theta-to-beta activity is statistically equivalent at both locations, except in its earliest phase. A very similar pattern of results was found for the activations resulting from left-ear stimulation, shown in Figures 3f and 3g. This only differs from the left-hemisphere data in the overlap between error bars at the 80-ms peak, although this analysis is based on only 5 participants. Indeed there were insufficient samples (providing only 4 degrees of freedom) to formally test differences in amplitude for statistical significance at the 0.05 alpha level. A further analysis of the FWHM of the event-related beamformer peaks (Barnes & Hillebrand, 2003) suggested an average of 17 mm (range 12-27) and 20 mm (range 13-20) for the theta-to-beta and gamma peaks respectively (no significant difference, Wilcoxon ranked pairs: $p > 0.05$). This suggested that although the peaks of sources can be distinguished appropriately based on the 5mm voxel grid used here, the uncertainty in the reconstructed source locations is such that the possibility of a degree of overlap between the sources cannot be excluded.

Reviewing sensor data, we observed that all seven of the participants in our left-hemisphere analysis who showed gamma activity also showed a small wave around 80 ms in the theta-to-beta band, although in one case this merged into the N1m. The mean (and standard deviation) latency of this response for left-ear stimulation was 72 ms (5 ms; n = 7) in the contralateral hemisphere and 77

ms (8 ms; n = 5) in the ipsilateral hemisphere. The mean (and standard deviation) latency of the response for right-ear stimulation was 81 ms (10 ms; n = 6) in the contralateral hemisphere and 80 ms (9 ms; n = 6) in the ipsilateral hemisphere. These latencies did not differ significantly from those for the gamma response shown in Table 1 (Wilcoxon ranked pairs, all $p > 0.1$). Yet they consistently failed to yield acceptable ER-beamformer activations in the theta-to-beta band, perhaps because of their relatively small amplitude, so their sources could not be modelled further. Figure 3e shows the Hilbert envelope of the gamma-band activity, and the time series of the theta-to-beta activity, both at the source of the peak gamma-band response. It can be seen that the rise in amplitude of the gamma response coincides with, or just precedes, the rise in amplitude of the lower-frequency response. However the phase-relationship between gamma and theta-to-beta activity was not robust when examining time series from individual virtual electrodes: in some cases the gamma preceded the rise of the low-frequency response and in other cases, *vice-versa*.

4 Discussion

Our data show that patterns of spectral power in specific frequency bands constitute an important distinguishing feature of the different components of the auditory evoked response, and localise to different regions of auditory cortex. In our volumetric images, the locations of peak gamma and peak theta-to-beta activity were spatially distinct in the hemisphere contralateral to stimulation, with the gamma responses falling more medial than the theta-to-beta responses (Figure 2). Our results also indicate that the activity in the theta-to-beta band is spatially widespread. Conversely, the gamma-band response appears to be more focal, and is significantly smaller at the location of the peak low-frequency response than at the location of the peak gamma response (Figs. 3c and 3d). These observations show that gamma-band response and the traditionally-defined N1m have temporally distinct onsets that correspond spatially with a hierarchical processing stream through auditory cortex.

4.1 Spatial Dissociation of Responses

The average localisation for both the gamma-band response and the theta-to-beta responses fell within or close to Heschl's gyrus. Importantly, gamma-band activity occurred in a significantly more medial position than theta-to-beta band activity. Primary auditory cortex has been described as having a set of core regions with at least 3 primary-like fields along the axis of the gyrus, with information flowing from medial to more lateral locations (Hackett, Preuss, & Kaas, 2001; Hackett, 2011). The mean localisations roughly corresponded to different cytoarchitectonic regions, suggesting that there are unique generators of gamma and theta-to-beta activity that are spatially distinct (although possibly overlapping) and may reflect stages of processing through the auditory system; this interpretation is also supported by the data in Figure 3d which show a significant difference between gamma-band amplitude at each source.

Gamma responses were localised to medial-lateral planes where Heschl's gyrus and the planum temporale are clearly observable. This location, particularly in the left hemisphere, corresponds to cytoarchitectonic region Te1.0 where there is a relatively thicker layer IV, i.e. receiving more thalamic input, than in the more medial Te1.1 and more lateral Te1.2 (Morosan et al., 2001). While cortex can generate gamma activity independently of thalamic input (Barth & MacDonald, 1996; Whittington, Traub, & Jefferys, 1995), the correspondence with a cytoarchitectonic region that receives relatively greater thalamic input than the other Te regions is consistent with suggestions that thalamic activity can also impact gamma activity (Barth & MacDonald, 1996; Metherate & Cruikshank, 1999). We also observed a small amount of gamma activity at the peak of the theta-to-beta activity, which could result from signal leakage in the beamformer model, or from overlapping sources – but alternatively it could have a neuronal origin. Chattering neurons in superficial layers of visual cortex can also generate gamma activity (Gray & McCormick, 1996) and it may be these neurons in auditory cortex that propagate gamma activity through auditory cortex (Metherate & Cruikshank, 1999). Future studies could further explore the independence of the gamma band responses at the two locations using modified beamformer approaches (Hui et al., 2010; Diwakar et al., 2011; Brookes et al., 2007).

Theta-to-beta responses were localised to more lateral temporal lobe regions, where the Heschl's gyrus morphology is highly variable across cases (Leonard, Puranik, Kuldau, & Lombardino, 1998), than the more medial primary gamma responses. The most probable cytoarchitectonic regions for theta-to-beta responses varied between hemispheres. In the left hemisphere, the response corresponded to cytoarchitectonic region Te1.2, where there is a relatively thicker layer III compared to Te1.0 and Te1.1 (Morosan et al., 2001). Layer II/III supragranular neurons demonstrate robust theta- and gamma-band activity in response to clicks (Lakatos, Chen, O'Connell, Mills, & Schroeder, 2007). We are cautious about interpreting the significance of localisation to Te1.2 in the left hemisphere though, because the right hemisphere theta-to-beta response was more likely in Te1.0. Moreover, relative layer thickness may not be the only, or most important, factor that determines the location of the peak gamma and theta-to-beta responses.

Cautious interpretation of the localisations is also warranted based on the high superior-inferior and anterior-posterior variability compared to the medial-lateral variability. The more lateral theta-to-beta responses may be particularly impacted by individual differences in sulcal/gyral morphology, as this will result in individual differences in the orientation of neurons with respect to the sensors and subsequently in localisation accuracy (Hillebrand & Barnes, 2002). Indeed, Heschl's gyrus morphology is increasingly variable across cases with increasingly lateral positions of the superior temporal gyrus (Leonard et al., 1998) and Heschl's gyrus morphology has been related to the magnitude of MEG responses to amplitude modulated tones (Schneider et al., 2002). Future studies with larger sample sizes may show that individual variance in Heschl's gyrus and Sylvian fissure morphology impacts the localisation of gamma and theta-to-beta responses. Individual differences in anatomy and potential registration error are less problematic for comparing the relative position of gamma and theta-to-beta responses using a within subjects design. Thus, we can more reliably conclude that theta-to-beta activity occurs laterally to the primary gamma responses to click stimuli.

4.2 Functional significance of activity in the gamma-band and theta-to-beta band

The spatial and temporal separation between the gamma-band response at 80-ms and the traditionally-defined N1m (i.e., the later component of the theta-to-beta response) is consistent with a functional distinction between their roles in the auditory responses. This result further strengthens an argument that MEG can be used to observe the processing of the clicks from medial to more lateral locations in auditory cortex.

Although the gamma activity described here is relatively late compared to the first signals arriving at the cortex following stimulation, which occur at around 20 ms (Lütkenhöner et al., 2003), evidence from intracortical recordings suggests that this frequency band is typically associated with bottom-up processes (Fontolan, Morillon, Liegeois-Chauvel, & Giraud, 2014), and its role in auditory thalamocortical coherence has previously been suggested (Ribary et al., 1991). While all areas in the core of Heschl's gyrus receive thalamic inputs, the peaks of our MEG signals will be centred at the spatial location where the bulk of activity originates. Again, the gamma response was more likely in Te1.0 where there is considerable thalamic input based on its relatively expanded layer IV.

Activity in the theta-to-beta band localises to more lateral areas of auditory cortex (Figure 2) and persists for longer than the gamma response (Figure 3), suggesting a role for this lower-frequency activity either in the flow of information along the auditory core and beyond, or top-down processes flowing towards A1. Evidence from intracortical depth recordings in A1 and auditory association cortex during speech stimuli has supported a functional distinction between gamma-band activity, reflecting bottom-up processes, and activity in lower frequency bands as a signature of top-down processing (Fontolan et al., 2014).

At the physiological level, oscillatory frequency will typically demonstrate an inverse relationship with the extent of neuronal recruitment (Buzsáki, 2006), possibly because when a rhythm is fast, only small groups of neurons can follow due to the limitations of conduction and synaptic delays. Our time series data imply that the source of the gamma-band activity may indeed be more focal than the source of the theta-to-beta activity. Although the FWHM analysis, which

showed no significant difference between the spatial extents of the beamformer reconstructions, does not seem to support this conclusion, it is important to realise that the extent of a peak in a beamformer image does not relate one-to-one to source extent. Indeed, very accurate models of cortical surface information are required for detailed assessment of source extent (Hillebrand & Barnes 2011)). Our analysis of virtual electrode timeseries data, along with the evidence from our confidence intervals, provide strong evidence for physiological dissociation between activity at these different sources. This provides a motivation for future detailed studies of MEG responses in auditory cortex, using beamformer methods with much higher numbers of trials to improve SNR and higher voxel resolution to allow finer dissociation between sources. Although the number of trials used in this study significantly exceeds that typically required to obtain an N1-P2 response in clinical electrophysiology (typically about 40-60 trials), it is possible that the accuracy and spatial selectivity of source localisations, as well as the consistency of timeseries data, would improve with greater numbers of trials. Further, while we did not specifically look for *induced* gamma activity in our analyses, none was observed – however. However with a significantly increased trial-count this may have emerged in the plots, or been localisable by using a standard dual-state (not event-related) beamformer analysis.

On average, the rise in gamma activity for the VEs was temporally co-incident with the rise of the 80-ms response in the lower frequency band, although this observation was not robust at the single-subject level, perhaps because of a lack of statistical power in the VE data. Coupling between induced theta rhythms and the envelope of bursting induced gamma activity has been well described in other brain areas (Canolty & Knight, 2010). Another way in which the two rhythms might be functionally related is through a common mechanism underpinning the generation of the evoked response. The 'Firefly model' (Burgess, 2012) provides a framework based on the phase-alignment of intrinsic oscillatory activity, which occurs through a slowing of rhythms that cascades from high to low frequencies. Thus, stimulus-related changes in the gamma band would be

expected to precede changes in lower frequencies. Individual differences in our data make it impossible to draw firm conclusions about the potential relationship between activity in these two frequency bands. Most notable was the fact that our dataset included two people who showed an evoked-gamma response in the absence of a traditionally-defined N1m response. This supports the view that the responses in the two frequency bands are functionally separate, although individual differences in the orientation of the respective neural generators could also account for this observation.

5 Conclusions

In summary, these data provide evidence that the oscillatory activity that underpins the auditory evoked response may contain important information about the physiological basis of the macroscopic signals recorded by MEG in response to auditory stimulation. Functional and spatial dissociations between activity in different frequency bands provide an opportunity to explore the dynamics of auditory processing and significantly supplement the information provided by traditional evoked response methods. More broadly, the results provide a richer understanding of auditory evoked responses that may be leveraged to understand where and when stimulus properties are typically processed and why people experience auditory processing difficulties.

6 Acknowledgements

The Wellcome Trust Laboratory for MEG Studies in the Aston Brain Centre is supported by a programme grant from the Dr Hadwen Trust. Author L.E.G. was supported by an Aston Brain Centre PhD studentship.

7 References

Adjamian, P., Worthen, S. F., Hillebrand, A., Furlong, P. L., Chizh, B. A., Hobson, A. R., … Barnes, G. R. (2009). Effective electromagnetic noise cancellation with beamformers and synthetic

gradiometry in shielded and partly shielded environments. *Journal of Neuroscience Methods*, *178*(1), 120–7.

Barnes, G.R. & Hillebrand, A. (2003). Statistical flattening of MEG beamformer images. *Human Brain Mapping*. 18(1), 1-12.

Barth, D. S., & MacDonald, K. D. (1996). Thalamic modulation of high-frequency oscillating potentials in auditory cortex. *Nature*, *383*(6595), 78–81.

Bartos, M., Vida, I., & Jonas, P. (2007). Synaptic mechanisms of synchronized gamma oscillations in inhibitory interneuron networks. *Nature Reviews. Neuroscience*, *8*(1), 45–56.

Brookes, M. J., Vrba, J., Robinson, S. E., Stevenson, C. M., Peters, A. M., Barnes, G. R., … Morris, P. G. (2008). Optimising experimental design for MEG beamformer imaging. *NeuroImage*, *39*(4), 1788–802.

Brookes, M.J., Stevenson, C.M., Barnes, G.R., Hillebrand, A., Simpson, M.I., Francis, S.T. & Morris, P.G. (2007) Beamformer reconstruction of correlated sources using a modified source model. *Neuroimage,* 34(4), 1454-65.

Burgess, A. P. (2012). Towards a Unified Understanding of Event-Related Changes in the EEG: The Firefly Model of Synchronization through Cross-Frequency Phase Modulation. *PLoS ONE*, *7*, e45630.

Buzsáki, G. (2006). Rhythms of the Brain. Oxford University Press.

Buzsáki, G., & Chrobak, J. J. (1995). Temporal structure in spatially organized neuronal ensembles: a role for interneuronal networks. *Current Opinion in Neurobiology*, *5*(4), 504–10.

Canolty, R. T., & Knight, R. T. (2010). The functional role of cross-frequency coupling. *Trends in Cognitive Sciences*, *14*(11), 506–15.

Cheyne, D., Bostan, A. C., Gaetz, W., & Pang, E. W. (2007). Event-related beamforming: a robust method for presurgical functional mapping using MEG. *Clinical Neurophysiology : Official Journal of the International Federation of Clinical Neurophysiology*, *118*, 1691–1704.

Crone, N. E., Boatman, D., Gordon, B., & Hao, L. (2001). Induced electrocorticographic gamma activity during auditory perception. Brazier Award-winning article, 2001. *Clinical Neurophysiology, 112*(4), 565–82.

Neuroimage. 2011 Jun 15;56(4):1918-28. doi: 10.1016/j.neuroimage.2011.03.042. Epub 2011 Apr 5.

Diwakar, M., Tal, O., Liu, T.T., Harrington, D.L., Srinivasan, R., Muzzatti, L., Song, T., Theilmann, R.J., Lee, R.R. & Huang, M.X. (2011). Accurate reconstruction of temporal correlation for neuronal sources using the enhanced dual-core MEG beamformer. *Neuroimage*, 56(4), 1918-28

Engel, A. K., & Singer, W. (2001). Temporal binding and the neural correlates of sensory awareness. *Trends in Cognitive Sciences*, *5*(1), 16–25.

Fontolan, L., Morillon, B., Liegeois-Chauvel, C., & Giraud, A.-L. (2014). The contribution of frequency-specific activity to hierarchical information processing in the human auditory cortex. *Nature Communications*, *5*, 4694.

Giraud, A.-L., & Poeppel, D. (2012). Cortical oscillations and speech processing: emerging computational principles and operations. *Nature Neuroscience*, *15*(4), 511–7.

Gray, C. M., & McCormick, D. A. (1996). Chattering cells: superficial pyramidal neurons contributing to the generation of synchronous oscillations in the visual cortex. *Science (New York, N.Y.)*, *274*(5284), 109–13.

Gray, C. M., & Singer, W. (1989). Stimulus-specific neuronal oscillations in orientation columns of cat visual cortex. *Proceedings of the National Academy of Sciences of the United States of America*, *86*(5), 1698–702.

Griffiths, T. D., Kumar, S., Sedley, W., Nourski, K. V, Kawasaki, H., Oya, H., … Howard, M. A. (2010). Direct recordings of pitch responses from human auditory cortex. *Current Biology : CB*, *20*(12), 1128–32.

Griffiths, T. D., & Warren, J. D. (2004). What is an auditory object? *Nature Reviews. Neuroscience*, *5*(11), 887–92.

Gross, J., Hoogenboom, N., Thut, G., Schyns, P., Panzeri, S., Belin, P., & Garrod, S. (2013). Speech rhythms and multiplexed oscillatory sensory coding in the human brain. *PLoS Biology*, *11*(12), e1001752.

Hackett, T. A. (2011). Information flow in the auditory cortical network. *Hearing Research*, *271*(1-2), 133–46.

Hackett, T. A., Preuss, T. M., & Kaas, J. H. (2001). Architectonic identification of the core region in auditory cortex of macaques, chimpanzees, and humans. *The Journal of Comparative Neurology*, *441*(3), 197–222.

Hillebrand, A., & Barnes, G. R. (2002). A quantitative assessment of the sensitivity of whole-head MEG to activity in the adult human cortex. *NeuroImage*, *16*(3 Pt 1), 638–50.

Hillebrand, A., & Barnes, G.R. (2011). Practical constraints on estimation of source extent with MEG beamformers. *NeuroImage* 54(4), 2732-2740.

Hillebrand, A., Singh, K. D., Holliday, I. E., Furlong, P. L., & Barnes, G. R. (2005). A new approach to neuroimaging with magnetoencephalography. *Human Brain Mapping*, *25*(2), 199–211.

Huang, M. X., Mosher, J. C., & Leahy, R. M. (1999). A sensor-weighted overlapping-sphere head model and exhaustive head model comparison for MEG. *Physics in Medicine and Biology*, *44*(2), 423–40.

Hui, H.B., Pantazis, D., Bressler, S.L. &. Leahy, R.M. (2010). Identifying true cortical interactions in MEG using the nulling beamformer. *Neuroimage*. 49(4), 3161.

Jacobson, G. P., & Fitzgerald, M. B. (1997). Auditory Evoked Gamma Band Potential in Normal Subjects, *52*, 44–52.

498 Jacobson, G. P., & Henderson, J. (1998). High Resolution Recording of Late Cortical Surface Potentials
499 N1 and Gamma Band Response (GBR), *94*, 87–94.

500 Kaiser, J., Hertrich, I., Ackermann, H., Mathiak, K., & Lutzenberger, W. (2005). Hearing lips: gamma-
501 band activity during audiovisual speech perception. *Cerebral Cortex*, *15*(5), 646–53.

502 Kumar, S., Stephan, K. E., Warren, J. D., Friston, K. J., & Griffiths, T. D. (2007). Hierarchical processing
503 of auditory objects in humans. *PLoS Computational Biology*, *3*(6), e100.

504 Laird, A. R., Robinson, J. L., McMillan, K. M., Tordesillas-Gutiérrez, D., Moran, S. T., Gonzales, S. M., …
505 Lancaster, J. L. (2010). Comparison of the disparity between Talairach and MNI coordinates in
506 functional neuroimaging data: validation of the Lancaster transform. *NeuroImage*, *51*(2), 677–
507 83.

508 Lakatos, P., Chen, C.-M., O'Connell, M. N., Mills, A., & Schroeder, C. E. (2007). Neuronal oscillations
509 and multisensory interaction in primary auditory cortex. *Neuron*, *53*(2), 279–92.

510 Lancaster, J. L., Tordesillas-Gutiérrez, D., Martinez, M., Salinas, F., Evans, A., Zilles, K., … Fox, P. T.
511 (2007). Bias between MNI and Talairach coordinates analyzed using the ICBM-152 brain
512 template. *Human Brain Mapping*, *28*(11), 1194–205.

513 Leonard, C. M., Puranik, C., Kuldau, J. M., & Lombardino, L. J. (1998). Normal variation in the
514 frequency and location of human auditory cortex landmarks. Heschl's gyrus: where is it?
515 *Cerebral Cortex*, *8*(5), 397–406.

516 Lisman, J. E. (1999). Relating hippocampal circuitry to function: recall of memory sequences by
517 reciprocal dentate-CA3 interactions. *Neuron*, *22*(2), 233–42.

518 Lisman, J. E., & Idiart, M. A. (1995). Storage of 7 +/- 2 short-term memories in oscillatory subcycles.
519 *Science*, *267*(5203), 1512–5.

520 Lütkenhöner, B., Krumbholz, K., Lammertmann, C., Seither-Preisler, A., Steinsträter, O., & Patterson,
521 R. D. (2003). Localization of primary auditory cortex in humans by magnetoencephalography.
522 *NeuroImage*, *18*(1), 58–66.

523 Metherate, R., & Cruikshank, S. J. (1999). Thalamocortical inputs trigger a propagating envelope of
524 gamma-band activity in auditory cortex in vitro. *Experimental Brain Research*, *126*(2), 160–74.

525 Mulert, C., Leicht, G., Pogarell, O., Mergl, R., Karch, S., Juckel, G., Moller, H.J. & Hegerl, U (2007)
526 Auditory cortex and anterior cingulate cortex sources of the early evoked gamma-band
527 response: relationship to task difficulty and mental effort. *Neuropsychologia* 45(10), 2294–
528 2306

529 Morosan, P., Rademacher, J., Schleicher, A., Amunts, K., Schormann, T., & Zilles, K. (2001). Human
530 primary auditory cortex: cytoarchitectonic subdivisions and mapping into a spatial reference
531 system. *NeuroImage*, *13*(4), 684–701.

532 Näätänen, R., & Picton, T. (1987). The N1 wave of the human electric and magnetic response to
533 sound: a review and an analysis of the component structure. *Psychophysiology*, *24*, 375–425.

Pantev C, Makeig S, Hoke M, Galambos R, Hampson S & Gallen C. (1991) Human auditory evoked gamma-band magnetic fields. *Proc Natl Acad Sci USA* 88(20), 8996–9000

Pantev, C. (1995). Evoked and induced gamma-band activity of the human cortex. *Brain Topography*, *7*(4), 321–330.

Polomac, N., Leicht, G., Nolte, G., Andreou, C., Schneider, T.R., Steinmann, S., Engel, A.K. and Mulert, C. (2015) Generators and connectivity of the early auditory evoked gamma band response. *Brain Topography* 28, 865-878.

Quraan, M. a, & Cheyne, D. (2010). Reconstruction of correlated brain activity with adaptive spatial filters in MEG. *NeuroImage*, *49*(3), 2387–400.

Rees, A., Green, G.G. & Kay, R.H. (1986) Steady-state evoked responses to sinusoidally amplitude-modulated sounds recorded in man. *Hearing Research*, 23(2), 123-33.

Ribary, U., Ioannides, A. A., Singh, K. D., Hasson, R., Bolton, J. P., Lado, F., … Llinás, R. (1991). Magnetic field tomography of coherent thalamocortical 40-Hz oscillations in humans. *Proceedings of the National Academy of Sciences of the United States of America*, *88*(24), 11037–41.

Robinson, S., & Vrba, J. (1999). Functional neuroimaging by synthetic aperture magnetometry (SAM). In T. Yoshimoto, M. Kotani, S. Kuriki, H. Karibe, & N. Nakasato (Eds.), *Recent Advances in Biomagnetism*. Tohoku, Japan: Tohoku University Press.

Ross, B., Borgmann, C., Draganova, R., Roberts, L.E. & Pantev, C. (2000) A high-precision magnetoencephalographic study of human auditory steady-state responses to amplitude-modulated tones. *J Acoust Soc Am*. 108(2), 679-91.

Schneider, P., Scherg, M., Dosch, H. G., Specht, H. J., Gutschalk, A., & Rupp, A. (2002). Morphology of Heschl's gyrus reflects enhanced activation in the auditory cortex of musicians. *Nature Neuroscience*, *5*(7), 688–94.

Sedley, W., Teki, S., Kumar, S., Overath, T., Barnes, G. R., & Griffiths, T. D. (2012). Gamma band pitch responses in human auditory cortex measured with magnetoencephalography. *NeuroImage*, *59*(2), 1904–11.

Singer, W. (1993). Synchronization of cortical activity and its putative role in information processing and learning. *Annual Review of Physiology*, *55*, 349–74.

Talairach, J., & Tournoux, P. (1988). *Co-planar stereotaxic atlas of the human brain.* New York: Theime.

Traub, R. D., Bibbig, A., LeBeau, F. E. N., Cunningham, M. O., & Whittington, M. A. (2005). Persistent gamma oscillations in superficial layers of rat auditory neocortex: experiment and model. *The Journal of Physiology*, *562*(Pt 1), 3–8.

Veen, B. D. Van, Drongelen, W. Van, Yuchtman, M., & Suzuki, A. (1997). Localization of Brain Electrical Activity via Linearly Constrained Minimum Variance Spatial Filtering. *IEEE Transactions on Biomedical Engineering*, *44*(9), 867–880.

Vrba, J., Anderson, G., Betts, K., Burbank, M., Cheung, T., Cheyne, D., … Sutherling, W. (1999). 151-Channel whole-cortex MEG system for seated or supine positions. In T. Yoshimoto, M. Kotani, S. Kuriki, H. Karibe, & N. Nakasato (Eds.), *Recent Advances in Biomagnetism* (pp. 93–96). Sendai: Tohoku University Press.

Vrba, J., & Robinson, S. E. (2001). Signal processing in magnetoencephalography. *Methods (San Diego, Calif.)*, *25*(2), 249–71. doi:10.1006/meth.2001.1238

Wang, X.-J. (2010). Neurophysiological and computational principles of cortical rhythms in cognition. *Physiological Reviews*, *90*(3), 1195–268.

Whittington, M. A., Traub, R. D., & Jefferys, J. G. (1995). Synchronized oscillations in interneuron networks driven by metabotropic glutamate receptor activation. *Nature*, *373*(6515), 612–5.

583

584 **Table 1**

Frequency Band	Left Ear Stimulation		Right Ear Stimulation	
	Contralateral Response	Ipsilateral Response	Contralateral Response	Ipsilateral Response
N1m	115 (12) n = 10	113 (10) n = 9	111 (11) n = 10	113 (15) n = 6
Gamma	79 (8) n = 8	78 (7) n = 6	76 (8) n = 8	77 (10) n = 5

585

586 Table 1 Legend: Mean (and standard deviation) latencies of the peak evoked responses, in ms, for
587 the N1m and gamma-band responses. There were no significant differences between contralateral
588 and ipsilateral latencies (Wilcoxon ranked pairs, $p > 0.05$).

589

590

591 **Table 2: Pseudo Z values**

Frequency Band	Left Ear Stimulation		Right Ear Stimulation	
	Contralateral Response	Ipsilateral Response	Contralateral Response	Ipsilateral Response
Theta-to-Beta (4-30 Hz)	16.2 (6.2) n = 10	6.4 (3.2) n = 4	13.0 (4.0) n = 9	10.2 (1.9) n = 7
Gamma (30-70 Hz)	14.2 (4.3) n = 6	9.2 (3.1) n = 5	12.3 (5.6) n = 8	11.6 (3.0) n = 7

592 **Table 2: legend**

593 Mean and standard deviation pseudo-Z values in the contralateral and ipsilateral hemispheres, in the
594 theta-to-beta and gamma frequency bands. Despite a trend for the ipsilateral pseudo-Z values to be
595 smaller, this was not statistically significant (Wilcoxon ranked pairs, $p > 0.05$).

596

597

598 **Figure Legends**

599

600 **Figure 1**

601 Figure 1 shows example evoked responses, taken from one MEG sensor located over the temporal
602 lobe contralateral to stimulation. In Fig. 1a, the response is bandpass-filtered between 1 and 30 Hz,
603 and in Fig. 1b the response is filtered between 30 and 70 Hz.

604

605 **Figure 2**

606 **Figures** 2a and 2b show mean and 95% confidence intervals for the ER beamformer peaks in the
607 theta-to-beta (dark blue) and gamma (light blue) frequency bands, plotted over the outline of
608 auditory cortex (Heschl's gyrus and planum temporale), traced from the 12mm slice of the Talairach
609 brain (Talairach & Tournoux 1988). Fig. 2a shows contralateral, i.e., right-hemisphere (n= 8 for each
610 frequency band) and ipsilateral activity (n = 7 for each band) resulting from left-ear stimulation,
611 while Fig. 2b shows contralateral (theta-to-beta, n = 10; gamma, n = 5) and ipsilateral (n = 4 for both
612 frequency bands) activity resulting from right-ear stimulation.

613

614 **Figure 3**

615 Figure 3 shows virtual electrode data for contralateral responses resulting from right-ear
616 stimulation, for the 7 participants who showed a response in both frequency bands. Figs. 3a and 3b
617 show wavelet spectrograms of activity at the source of the theta-to-beta activity and gamma activity
618 respectively. Figs. 3c and 3d show evoked response time series at the sources of the theta-to-beta
619 activity and gamma activity, filtered in the low frequency band (3c) and gamma-band (3d),
620 respectively. These are scaled as a function of 1 standard deviation of pre-stimulus activity in each
621 individual and averaged. Error bars show standard deviations of the peak amplitudes. Figure 3e
622 shows the relative timing of the activity in each frequency at the location of the peak gamma
623 response. The Hilbert envelope of the gamma activity, shown in red, is plotted with the slow (theta-

624 to-beta) response at the same location in Figure 3e. Figures 3f and 3g show the similar plots to 3c

625 and 3d, using the data from left ear stimulation and sources in the right hemisphere.

626

a

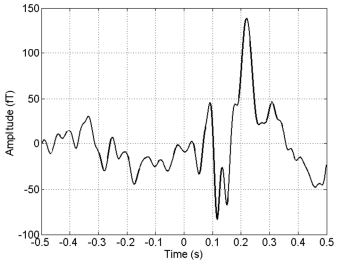

b

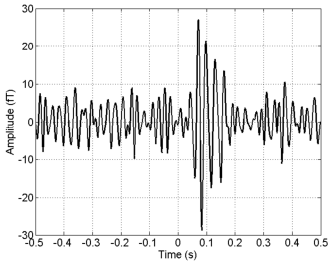

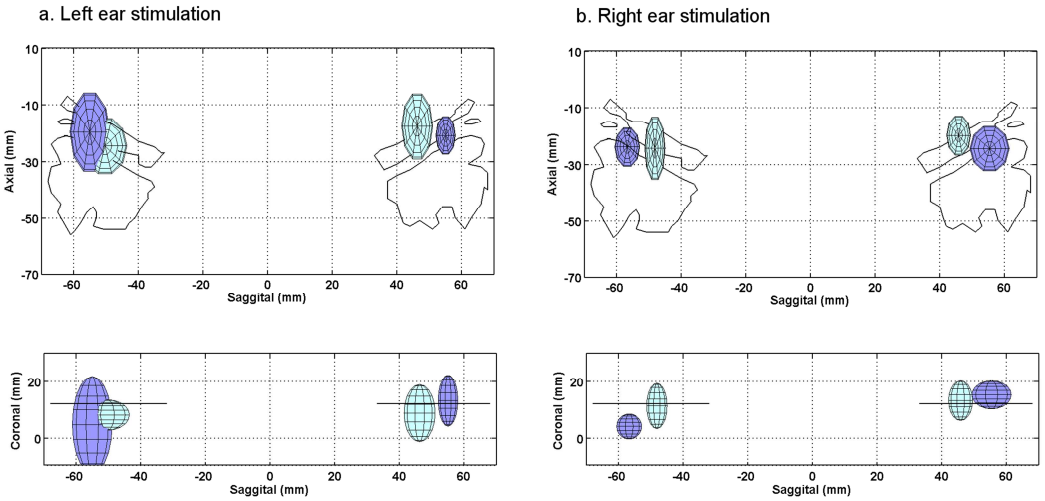
a. Left ear stimulation
b. Right ear stimulation
Axial (mm)
Saggital (mm)
Coronal (mm)
Saggital (mm)
10
-10
-30
-50
-70
20
0
-60
-40
-20
0
20
40
60

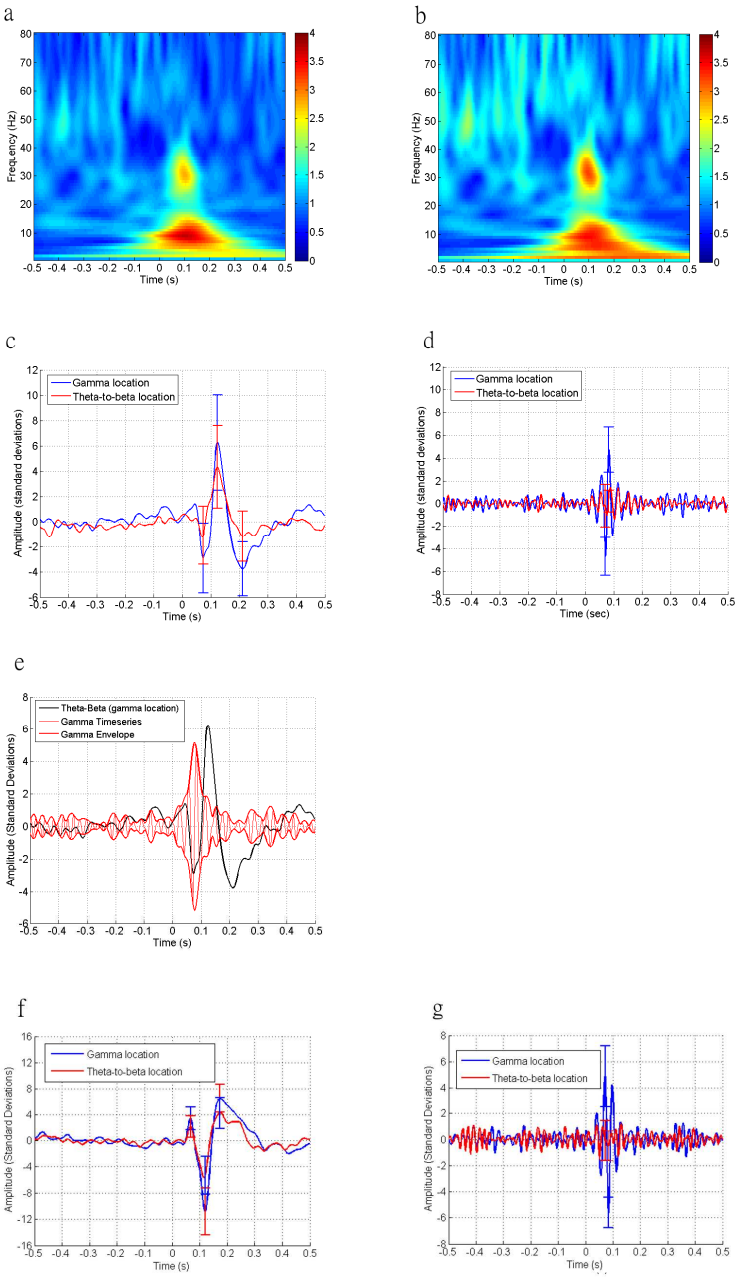
a
Frequency (Hz)
Time (s)
b
Frequency (Hz)
Time (s)
c
Gamma location
Theta-to-beta location
Amplitude (standard deviations)
Time (s)
d
Gamma location
Theta-to-beta location
Amplitude (standard deviations)
Time (sec)
e
Theta-Beta (gamma location)
Gamma Timeseries
Gamma Envelope
Amplitude (Standard Deviations)
Time (s)
f
Gamma location
Theta-to-beta location
Amplitude (Standard Deviations)
Time (s)
g
Gamma location
Theta-to-beta location
Amplitude (Standard Deviations)
Time (s)

Highlights

- We compare the auditory cortical N1m and evoked gamma responses using MEG
- Gamma-band activity originates more medially in auditory cortex than the N1m
- Gamma activity is earlier and spatially distinct from N1m responses
- Data are consistent with separate origins and functional roles of these responses